Lawrence Berkeley National Laboratory
LBL Publications

Title
Rotational coherence dominates early-time dynamics and produces long-time revivals in the S2 state of azulene

Permalink
https://escholarship.org/uc/item/9h63655q

Journal
The Journal of Chemical Physics, 164(15)

ISSN
0021-9606

Authors
Zhan, Jie
Lemmens, Alexander K
Ahmed, Musahid
et al.

Publication Date
2026-04-21

DOI
10.1063/5.0321301

Copyright Information
This work is made available under the terms of a Creative Commons Attribution License, available at https://creativecommons.org/licenses/by/4.0/

Peer reviewed

eScholarship.org Powered by the California Digital Library
University of California

Rotational Coherence Dominates Early-Time Dynamics and Produces Long-Time Revivals in the S_2 State of Azulene

Jie Zhan,[1] Alexander K. Lemmens,[2] Musahid Ahmed,[2] and Melanie A. R. Reber[1]
[1)] *Department of Chemistry, University of Georgia, Athens, GA*
[2)] *Chemical Science Division, Lawrence Berkeley National Laboratory, Berkeley, CA*

(*Electronic mail: mreber@uga.edu)

(*Electronic mail: MAhmed@lbl.gov)

(Dated: 01/06/2026)

The ultrafast dynamics of azulene have been debated for decades, with reported picosecond decay constants variously attributed to intramolecular vibrational redistribution (IVR), internal conversion, or rotational dephasing. Using polarization and femtosecond time-resolved Resonance Enhanced Multi-photon Ionization Spectroscopy with a nanosecond delay window, we disentangle this long-standing inconsistency and show that the early 2–5 ps decay component arises entirely from rotational dephasing of an excited-state wavepacket. Identical time constants extracted from the decay of the parallel signal and rise of the perpendicular signal across multiple vibronic origins provide an unambiguous rotational anisotropy signature, eliminating the need for IVR-based interpretations. Extending the measurement window to 1.3 ns reveals well-structured J-type and C-type rotational coherence revivals in S_2 azulene on top of the well-documented fluorescence decay, demonstrating that both the short- and long-time dynamics contain information about the coherent rotational dynamics. These results show that azulene, and by extension polycyclic aromatic hydrocarbons (PAH), can sustain structured rotational coherence deep into the nanosecond regime, positioning PAHs as model systems for quantum-coherent wavepacket dynamics and providing a framework for probing coherence, decoherence, and rotational control in electronically rich molecular systems.

arXiv:2601.06003v1 [physics.chem-ph] 9 Jan 2026

I. INTRODUCTION

Azulene is a 10-π-electron aromatic molecule distinguished by its bright S_2 excited state and dark S_1 state, a consequence of its well-known anti-Kasha behavior.[1] Although its femtosecond dynamics have been extensively investigated in condensed phases,[2–6] only a limited number of studies[7–10] have examined S_2 dynamics in molecular beams with femtosecond to picosecond time resolution. These gas-phase studies report notable differences in both the observed decay behavior and its interpretation.

Azulene's S_2 dynamics are often described by two principal time constants: one in the picosecond regime and another in the nanosecond regime. In 1987, Demmer et al.[10] reported a 2 ns decay attributed to radiative relaxation of S_2, along with an initial sub-30 ps decay that they assigned to intramolecular vibrational redistribution (IVR). This interpretation was later adopted by Diau et al.[9] in a femtosecond time-resolved mass-spectrometry experiment, where a 350 fs decay component was observed and described as consistent with the IVR timescale reported by Demmer et al.[10] A later study by Raffael et al.[7] argued instead that the picosecond component arises from rotational dephasing, based on time-resolved photoionization measurements comparing parallel and perpendicular pump–probe geometries. They reported dephasing times of 1.7–4.3 ps for seeded versus pure molecular beams, though their data extended only to 3 ps and did not include full kinetic fits. In a companion study, the same group attempted to observe rotational coherence revivals at longer delays but did not detect them.[8] In this work, we address the inconsistencies in the reported early-time dynamics of S_2 azulene by conducting experiments using pump energies that selectively access $S_2 \rightarrow S_0$ vibronic transitions. This approach provides vibrational-state specificity together with femtosecond time resolution extending into the nanosecond regime, allowing us to examine both the origin of the picosecond decay and the presence of rotational coherence revivals in addition to the S_2- S_0 fluorescence associated with the S_2 population decay. Parallel, perpendicular, and magic angle pump–probe polarization schemes were employed to verify the role of rotational dephasing in the early-time signal. By combining femtosecond excitation with a nanosecond delay stage, we also investigated longer-time dynamics up to 1.3 ns and analyzed rotational coherence in this extended time window for the first time.

II. METHODS

A. Experimental

The experiments were conducted using a home-built Time-Resolved Resonance-Enhanced Multiphoton Ionization (TR-REMPI) spectrometer at Lawrence Berkeley National Laboratory (LBNL).[11] Laser pulses from a Coherent Monaco Yb:fiber laser were split into separate pump and probe beams. The probe beam, comprising 33% of the seed, was frequency-tripled to 345 nm via third-harmonic generation, while the remaining 67% was directed to a Light Conversion Opera-HP optical parametric amplifier to generate the pump wavelengths. A motorized delay stage on the probe arm enabled scans extending past 1 ns. Pump wavelengths from 348.2 to 329.1 nm (3.56 to 3.77 eV) were used in the experiments. The pump and probe beams were focused and intersected with the molecular beam in the interaction region.

Solid azulene (Sigma-Aldrich, 99%) was placed in a

stainless-steel reservoir heated to 350 K, with 450 Torr of argon flowing over it. The resulting mixture was expanded through a 50 μm nozzle into vacuum to form a supersonic molecular beam. After passing through a 2 mm skimmer, the beam entered the interaction region where it overlapped with the pump and probe. Azulene has an ionization energy of 7.4 eV; to achieve 1+2' ionization, a tightly focused probe beam was used in combination with a weakly focused pump beam. Ions were collected using a microchannel plate (MCP) detector coupled to a time-of-flight mass spectrometer. The signal intensity is obtained by integrating the mass spectrum over a window centered on the target mass. The instrument response function has a time resolution of 350 fs and a 1.2 nm FWHM as determined from the observed minimum linewidths, allowing both frequency-resolved and time-resolved measurements to be obtained.

B. Molecular Structure Calculations

Calculations of the S_0 and S_2 states of azulene were performed using Gaussian16[12] at the CAM-B3LYP/6-311G(d,p) level of theory. The ground-state geometry was optimized using DFT, and the excited-state analysis was carried out using TD-DFT. All optimizations were constrained to C_{2v} symmetry. Franck–Condon and Herzberg–Teller (FCHT) analyses were subsequently performed using Gaussian16, and stick spectra were generated from the computed vibronic intensities. The electronic-structure methodology follows the level of theory employed by Palmer et al.[13], while all FCHT calculations and spectral generation were performed independently in this work. The resulting spectra are shown in Figure 1.

C. Time Resolved Data Model

The time-dependent REMPI signal contains several contributing processes, all of which are included in the kinetic model. These processes are: the instrument response function, a coherent artifact, a fast decay component, and a slow decay component. For delays up to 20 ps, the kinetics for both parallel and perpendicular pump–probe polarizations are adequately described by a single-exponential process. The model consists of a Gaussian term with width, ω_δ, that accounts for the coherent artifact (CA), followed by a fast component representing the dynamics within the first 20 ps with a time constant τ. This fast component appears as a single-exponential decay for the parallel configuration and as a corresponding rise for the perpendicular configuration, which represents a phenomenological fit as the rotational dephasing is not strictly exponential. A slow component associated with fluorescence with a lifetime exceeding 1 ns, is also included; with S and d as the fit parameters. The parameter t_0 denotes the temporal overlap of the pump and probe pulses and defines time zero and each component has an intensity scaling factor, P_n.

$$\mathrm{CA} = \frac{P_1}{\sqrt{2\pi}\, w_\delta} \exp\left[-\frac{(t-t_0)^2}{2w_\delta^2}\right] \tag{1}$$

$$\text{Fast Component (Parallel)} = P_2 e^{-(t-t_0)/\tau}, \quad \text{for } t \geq t_0 \tag{2}$$

$$\text{Fast Component (Perpendicular)} = P_2(1-e^{-(t-t_0)/\tau}), \quad \text{for } t \geq t_0 \tag{3}$$

$$\text{Slow Component} = S \times (t-t_0) + d, \quad \text{for } t \geq t_0 \tag{4}$$

The total kinetics model is therefore:

$$\text{Total Signal} = (\mathrm{CA} + \text{Fast Component} + \text{Slow Component}), \quad \text{for } t \geq t_0 \tag{5}$$

In ultrafast pump–probe measurements, the minimum achievable time resolution is determined by the instrument response function (IRF), which quantifies the combined temporal response of the excitation and detection system. The measured IRF is well described by a Gaussian function with a width, ω_{irf}:

$$\mathrm{IRF}(t, \omega_{irf}) = \frac{1}{\sqrt{2\pi}\,\omega_{\mathrm{irf}}} \exp\left[-\frac{(t-t_0)^2}{2\omega_{\mathrm{irf}}^2}\right]. \tag{6}$$

The raw data are fit to the convolution of the kinetic model and the IRF (Eq. 7).

$$I(t) = \left\{ CA + signal \cdot H(t-t_0) \right\} \otimes \mathrm{IRF}(t, \omega_{irf}), \qquad H(t-t_0) = \begin{cases} 1, & t \geq t_0, \\ 0, & t < t_0. \end{cases} \tag{7}$$

The Heaviside step function $H(t-t_0)$ ensures that the kinetic terms contribute only for $t \geq t_0$. All time-dependent data were fit to this model using a non-linear least-squares routine.

III. RESULTS AND DISCUSSION

Figure 1 shows the 1+2' REMPI spectrum together with the simulated Franck–Condon and Herzberg–Teller (FC–HT) stick spectrum of azulene. The probe photon energy was fixed at 3.59 eV while pump photon energies were scanned from 3.5 to 3.9 eV. The calculated spectrum was generated at 0 K and shifted by -0.091 eV to align with the experimental results, showing good agreement between experiment and theory. Vibronic assignments follow the notation $|S_0\ vibrational\ state> \rightarrow |S_2\ vibrational\ state>$, with the vibrational quanta indicated as superscripts.

The origin of the experimental ($|0> \rightarrow |0>$) transition occurs at 3.561 eV (28719 cm^{-1}, 348.2 nm), in good agreement with the previously reported value of 28757 cm^{-1} (3.565

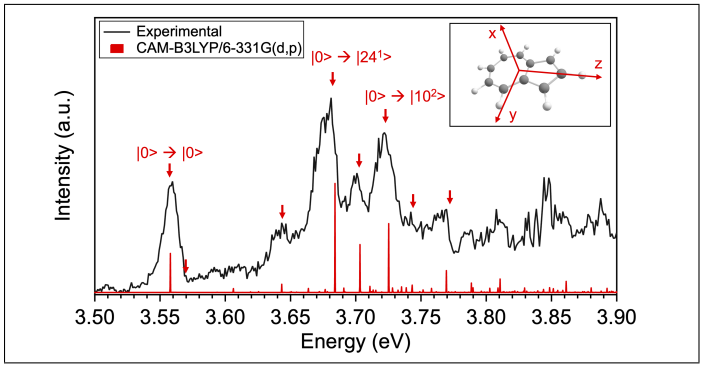

FIG. 1. Measured REMPI Spectrum and calculated Franck-Condon Herzberg-Teller spectrum at 0 K. The FWHM of the calculated spectrum is 1 cm^{-1} and shifted to a lower energy by 0.091 eV. This work specifically studied the photon energies indicated by the red arrows. The inset shows the structure and principle axes of azulene.

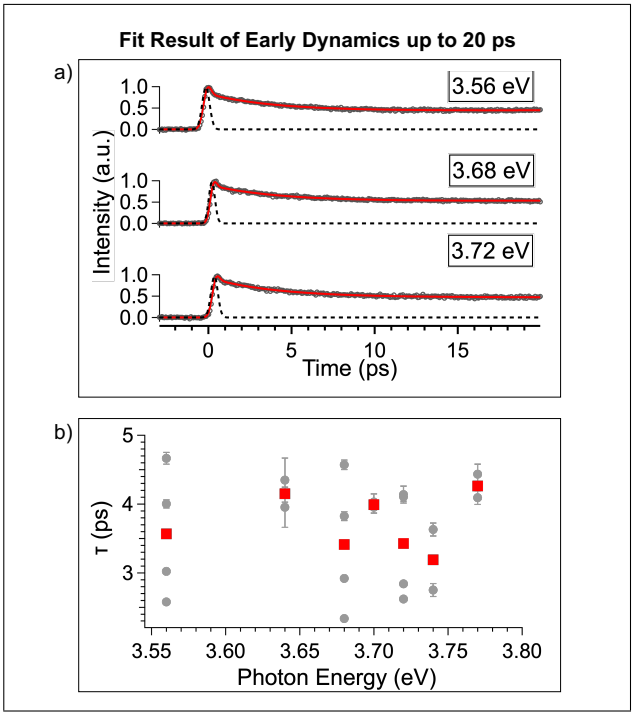

FIG. 2. a) Normalized decay kinetics (grey markers) measured for early time dynamics with pump energy of 3.56 eV, 3.68 eV and 3.72 eV. Red curve shows exponential fit result and the black dashed traces are the fitted IRF. b) Time constants from the fit results for all seven pump energies (grey circles with error bars), The average time constants of the early time dynamics (red squares).

eV, 347.7 nm).[10] Based on the REMPI spectrum, eight pump photon energies corresponding to distinct vibronic transitions were selected for time-resolved measurements under the 1+2' scheme. Photon energies above 3.77 eV were excluded because the sum of a pump and probe photon exceeds the ionization energy of azulene, placing those conditions outside the 1+2' regime. Ultrafast REMPI experiments were therefore conducted at 3.56, 3.57, 3.64, 3.68, 3.70, 3.72, 3.74, and 3.77 eV, as indicated by the red arrows in Figure 1. Pump Seven of these energies are resonant with $|S_0 >\rightarrow |S_2 >$ vibronic transitions, while one (3.57 eV) is off-resonance. The selected energies sample both isolated vibronic bands and regions with overlapping transitions.

Figure 2a shows single-exponential fits to the early-time decay at 3.56, 3.68, and 3.72 eV under parallel pump–probe polarization. The early time decay of off-resonance pump energy (3.57 eV) is showed in Figure S1. Figure 2b summarizes the extracted fast-decay time constants for all pump energies; complete fit results are provided in the Supporting Information (Table S1). Gray circles represent individual fitted time constants with their corresponding uncertainties in the fit, while the red squares denote the average value at each wavelength. This early-time constant is attributed to the initial dephasing of rotational coherence.[14]

When molecules are excited by a polarized pulse, those with transition dipole moments aligned along the polarization axis are preferentially excited. As the molecules freely rotate, this initial alignment rapidly dephases, giving rise to the picosecond-scale decay. The intensity of the rotational coherence signal I depends on time, the excitation and detection polarizations, the orientation of the relevant transition dipole moments, and the rotational temperature of the sample.[15] No systematic trend in the extracted time constants was observed for photon energies above the vibronic origin. Additional evidence supporting the rotational-dephasing assignment comes from the perpendicular pump–probe configuration, in which the signal exhibits a rise rather than a decay (Figure 3a). The fit results for the parallel and perpendicular pump-probe configurations at the same molecular beam parameters are provided in Table S2. Measurements were also performed using the magic-angle pump–probe configuration (Figure S2) to confirm the absence of decay mechanisms other than rotational coherence. This behavior is characteristic of rotational dynamics and has been observed previously by Raffael et al.;[7] however, they reported a sub-1-ps dephasing time, likely due to the higher rotational temperature of their molecular beam.[14]

We also calculated the rotational anisotropy (Figure S3) for the initial several picoseconds at pump photon energies of 3.56, 3.78, and 3.72 eV. In all three cases, the anisotropy has a value of approximately 0.2 at time zero, consistent with the results reported by Raffael et al.[7] and significantly lower than the theoretical maximum of 0.4.[15] This reduction in anisotropy is physically meaningful. Thermal averaging over multiple rovibronic transitions, each with different transition dipole orientations, would reduce the initial anisotropy. An additional contribution may arise from a mismatch between the vibronic transition dipole addressed by the pump and the photoionization dipole that governs the probe, which would also prevent the anisotropy from reaching its theoretical limit of 0.4.[16]

To further confirm the identity of the initial decay constant and to test whether any part of it could be attributed to IVR, we extended the ultrafast REMPI measurements to delays of 1.3 ns, as shown in Figure 3b. The three scans correspond to pump photon energies of 3.56, 3.68, and 3.72 eV, with a step size of 3 ps. The long-time decay is characterized by a

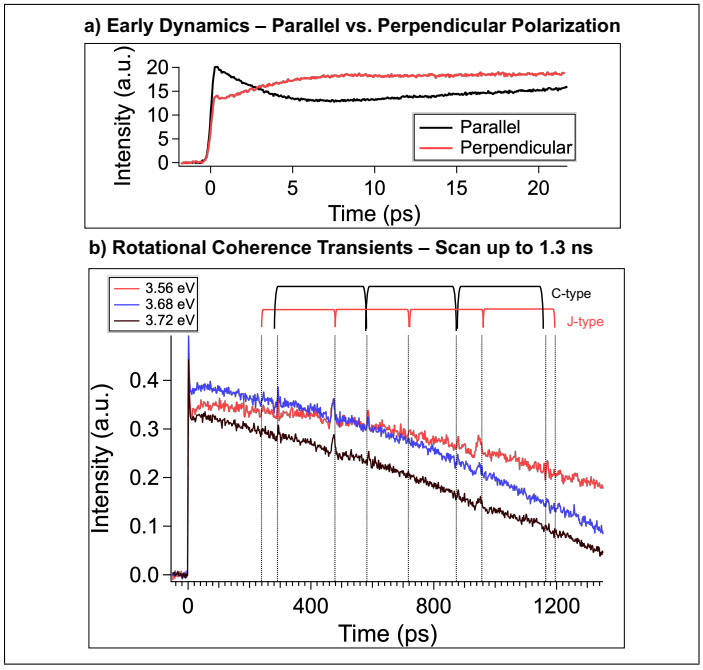

FIG. 3. a) Decay kinetics pumped at 3.56 eV with different pump polarization. b) Normalized Time-Resolved REMPI spectra pumped at 3.56, 3.68 and 3.72 eV scanned up to 1.3 ns with J type and C type rotational coherence transients labeled. J type transients labeled in red indicating a positive signal and blue indicating a negative signal. The results are calculated within the near-prolate top approximation.

time constant of 1482 ± 73 ps, which we assign to the S_2 fluorescence lifetime, in agreement with the value reported by Demmer et al.[10] At extended nanosecond delays, we also observe a recurring signal associated with rotational coherence in S_2 azulene, which is reported here for the first time.

Azulene is a near-prolate asymmetric top, characterized by Ray's asymmetry parameter $\kappa = -0.61$. Our analysis therefore follows previous treatments of near-symmetric top species.[14] The S_2 state of azulene exhibits rotational constants that satisfy $(B+C) \approx A \gg (B-C)$ as expected for a near-prolate top. For the dominant vibronic transitions investigated here, the transition dipole moment lies along the a axis, also denoted as the z axis and taken as the principal axis of the molecule. On this basis, we assign the labeled features in the time-resolved data as J-type and C-type transients.[17]

J-type transients can arise for nearly any orientation of the transition dipole moment relative to the principal axes. They correspond to coherences between states with different total angular momentum but the same projection quantum number ($|\Delta J| = 1,2 \;\; |\Delta K| = 0$).[18] These transients persist even as the rotor becomes asymmetric. For asymmetric molecules such as azulene, J-type revivals occur at approximately $t = 1/2(B+C)$ and exhibit alternating signal polarity.[17]

C-type transients, by contrast, are "asymmetry transients". They arise from $\Delta J = 2,\ \Delta K = 0$ rovibronic coherences[18] and appear sharper in the time domain than the main J-type peaks.[17] C-type transients are characteristic of prolate-like species when the transition moment lies along the a axis, which applies to all three vibronic transitions excited in this experiment. The observed transients therefore show a strong correlation with the transition dipole moment of the molecule. For the 3.56 eV ($|0> \rightarrow |0>$ and 3.68 eV ($|0> \rightarrow |24^1>$) transitions, the transition dipole moment derivative is oriented along the a axis, whereas the 3.72 eV transition $|0> \rightarrow |10^2>$ has its transition dipole moment derivative along the c axis (x axis). As a result, the effective transition dipole moments for these three bands are distributed between the a and c axes. C-type transients are revived at approximately $t = 1/4C$.[17]

TABLE I. **Revival times for J-type and C-type signals (ps)**

Type	Revival times (ps)
J-type	239.2, 478.3, 717.5, 956.7, 1195.8
C-type	291.2, 582.4, 873.6, 1164.8

The J-type and C-type transients of excited-state azulene were calculated using the S_2 rotational constants from Semba et al.,[19] following the approach outlined in Ref. 14. The calculated revival times are listed in Table I. For the three pump energies shown in Figure 3b, the recurring experimental features appear at approximately the same time delays. This indicates that the rotational constants of the final vibrational states accessed at these energies are very similar to those of the S_2 origin, and that their geometries are therefore comparable. At 3.72 eV, the rotational coherence revivals display a weaker C-type contribution, consistent with the transition dipole moment not being purely aligned along the a axis. No A-type transients are observed, implying that the derivative of the transition dipole moment along the remaining principal axis makes only a minor contribution to the total transition dipole. The J-type revival times at the three pump energies are observed to shift to slightly earlier delays, as expected for asymmetric tops.[14] For asymmetric-top molecules, J-type transients at $t = (2m+1)/2(B+C)$, $(m = 0,1,2...)$ lose intensity more rapidly,[15,17,20] in agreement with our observations. With these assignments in hand, we use the widths of the J-type and C-type revivals to model the initial decay.[21] The early-time decay can be reproduced by summing the dephasing of both sets of transients (Figure S4), ruling out IVR as the decay mechanism.

IV. CONCLUSION

The present study provides a unified interpretation of S_2-state dynamics in azulene by combining polarization-resolved femtosecond TR-REMPI measurements with extended nanosecond detection. The widely reported 2–5 ps decay observed in earlier studies is shown here to originate from rotational dephasing rather than intramolecular vibrational redistribution. This assignment is supported by the identical time constants extracted from the decay of the parallel signal and the rise of the perpendicular signal across several vibronic transitions, which together constitute a clear rotational anisotropy signature. This conclusion is further confirmed by the presence of rotational revivals at long times. This result resolves long-standing inconsistencies in the azulene literature,

where variations in beam temperature and excitation conditions produced apparently conflicting "IVR timescales."

Extending the measurement window to 1.3 ns reveals structured rotational coherence in S_2 azulene, manifested as J-type and C-type transient features whose timings are consistent with those expected for a near-prolate asymmetric top. The recurrence structure connects continuously to the early-time anisotropy decay, indicating that the short- and long-time behaviors arise from a single underlying rotational coherence. Differences in the strength of C-type contributions among the probed vibronic bands are explained by the orientation of their transition dipole moment derivatives, highlighting the sensitivity of rotational coherence to vibronic character.

These findings establish that excited-state azulene supports rotational coherence over hundreds of picoseconds and into the nanosecond regime, behavior not previously documented for this prototypical aromatic chromophore. This refined picture of S_2 dynamics clarifies the mechanistic origin of both the early picosecond decay and the late-time recurrence structure, and it provides a framework for reinterpreting prior ultrafast measurements on azulene and related PAHs.

Looking ahead, the observation of long-lived rotational coherence in an electronically excited PAH suggests several promising directions. Measurements across additional vibronic transitions could map structural changes of vibronic states along with associated changes in lifetimes or rotational dephasing dynamics. Complementary modeling of asymmetric-top rotational dynamics, or the use of temperature-controlled molecular beams, could quantify the role of rotational temperature and asymmetry splitting in shaping the observed transients. Finally, extending similar measurements to larger PAHs would test how molecular size, rigidity, and π-electron delocalization influence the persistence and structure of rotational coherence.

ACKNOWLEDGMENTS

SL & MA are supported by the Gas Phase Chemical Physics Program, in the Chemical Sciences Geosciences and Biosciences Division of the Office of Basic Energy Sciences of the U.S. Department of Energy under Contract No. DE-AC02-05CH11231. JZ & MR acknowledge support from the National Science Foundation CAREER Program under Award Number 2340180.

DATA AVAILABILITY STATEMENT

The data that support the findings of this study are available from the corresponding author upon reasonable request.

CREDIT

The following article has been submitted for peer-review publication. After it is published, it will be found at the journal website.

REFERENCES

[1] D. Dunlop, L. Ludvikova, A. Banerjee, H. Ottosson, and T. Slanina, "Excited-state (anti) aromaticity explains why azulene disobeys Kasha's rule," J. Am. Chem. Soc. **145**, 21569–21575 (2023).

[2] P. Wirth, S. Schneider, and F. Dörr, "Ultrafast electronic relaxation in the S_1 state of azulene and some of its derivatives," Chem. Phys. Lett. **42**, 482–487 (1976).

[3] A. Wurzer, S. Lochbrunner, and E. Riedle, "Highly localized vibronic wavepackets in large reactive molecules," Appl. Phys. B **71**, 405–409 (2000).

[4] L. Ciano, P. Foggi, and P. R. Salvi, "The dynamics of azulene S_2 state characterised by femtosecond transient absorption spectroscopy," J. Photochem. Photobiol., A **105**, 129–134 (1997).

[5] H.-P. Solowan, P. Malý, and T. Brixner, "Direct comparison of molecular-beam vs liquid-phase pump–probe and two-dimensional spectroscopy on the example of azulene," J. Chem. Phys. **157**, 044201 (2022).

[6] Y. Sawada, A. Takada, K. Onda, K. Miyata, Y. Sasaki, and N. Kimizuka, "Ultrafast nonradiative decay from higher-lying excited states in azulene-dimers," Phys. Chem. Chem. Phys. **27**, 19677–19683 (2025).

[7] K. Raffael, V. Blanchet, B. Chatel, G. Turri, B. Girard, I. A. Garcia, I. Wilkinson, and B. J. Whitaker, "Time-dependent photoionization of azulene: Optically induced anistropy on the femtosecond scale," Chem. Phys. Lett. **460**, 59–63 (2008).

[8] V. Blanchet, K. Raffael, G. Turri, B. Chatel, B. Girard, I. A. Garcia, I. Wilkinson, and B. J. Whitaker, "Time-dependent photoionization of azulene: Competition between ionization and relaxation in highly excited states," J. Chem. Phys. **128**, 164318 (2008).

[9] E. W.-G. Diau, S. De Feyter, and A. H. Zewail, "Direct observation of the femtosecond nonradiative dynamics of azulene in a molecular beam: The anomalous behavior in the isolated molecule," J. Chem. Phys. **110**, 9785–9788 (1999).

[10] D. R. Demmer, J. W. Hager, G. W. Leach, and S. C. Wallace, "Picosecond dynamics of intramolecular vibrational redistribution in the S_2 state of jet-cooled azulene," Chem. Phys. Lett. **136**, 329–334 (1987).

[11] A. K. Lemmens, N. Dias, H. G. Tuckman, E. Neuscamman, and M. Ahmed, "Vibrations and the passage through a diabolic point in the anthracene dimer," J. Chem. Phys. **163**, 024318 (2025).

[12] M. J. Frisch, G. W. Trucks, H. B. Schlegel, G. E. Scuseria, M. A. Robb, J. R. Cheeseman, G. Scalmani, V. Barone, G. A. Petersson, H. Nakatsuji, X. Li, M. Caricato, A. V. Marenich, J. Bloino, B. G. Janesko, R. Gomperts, B. Mennucci, H. P. Hratchian, J. V. Ortiz, A. F. Izmaylov, J. L. Sonnenberg, D. Williams-Young, F. Ding, F. Lipparini, F. Egidi, J. Goings, B. Peng, A. Petrone, T. Henderson, D. Ranasinghe, V. G. Zakrzewski, J. Gao, N. Rega, G. Zheng, W. Liang, M. Hada, M. Ehara, K. Toyota, R. Fukuda, J. Hasegawa, M. Ishida, T. Nakajima, Y. Honda, O. Kitao, H. Nakai, T. Vreven, K. Throssell, J. A. Montgomery, Jr., J. E. Peralta, F. Ogliaro, M. J. Bearpark, J. J. Heyd, E. N. Brothers, K. N. Kudin, V. N. Staroverov, T. A. Keith, R. Kobayashi, J. Normand, K. Raghavachari, A. P. Rendell, J. C. Burant, S. S. Iyengar, J. Tomasi, M. Cossi, J. M. Millam, M. Klene, C. Adamo, R. Cammi, J. W. Ochterski, R. L. Martin, K. Morokuma, O. Farkas, J. B. Foresman, and D. J. Fox, "Gaussian~16 Revision C.01," (2016), gaussian Inc. Wallingford CT.

[13] M. H. Palmer, N. C. Jones, S. V. Hoffmann, R. A. Aitken, M. Coreno, M. de Simone, C. Grazioli, and I. L. J. Patterson, "The excited states of azulene: A study of the vibrational energy levels for the lower $\pi\pi^*$-valence states by configuration interaction and density functional calculations, and theoretical studies of the Rydberg states," J. Chem. Phys. **157**, 154307 (2022).

[14] P. M. Felker and A. H. Zewail, "Molecular structures from ultrafast coherence spectroscopy," in *Femtosecond Chemistry* (John Wiley & Sons, Ltd, 1994) Chap. 5, pp. 193–260, https://onlinelibrary.wiley.com/doi/pdf/10.1002/9783527619436.ch5.

[15] P. M. Felker and A. H. Zewail, "Purely rotational coherence effect and time-resolved sub-Doppler spectroscopy of large molecules. I. Theoretical," J. Chem. Phys. **86**, 2460–2482 (1987).

[16] N. Scherer, L. Khundkar, T. Rose, and A. Zewail, "Sub-Doppler measurement of excited-state rotational constants and rotational coherence by pi-

cosecond multiphoton ionization mass spectrometry," J. Phys. Chem. **91**, 6478–6483 (1987).

[17] P. W. Joireman, L. L. Connell, S. M. Ohline, and P. M. Felker, "Characterization of asymmetry transients in rotational coherence spectroscopy," J. Chem. Phys. **96**, 4118–4130 (1992).

[18] P. M. Felker, "Rotational coherence spectroscopy: studies of the geometries of large gas-phase species by picosecond time-domain methods," The Journal of Physical Chemistry **96**, 7844–7857 (1992).

[19] Y. Semba, K. Yoshida, S. Kasahara, C.-K. Ni, Y.-C. Hsu, S. H. Lin, Y. Ohshima, and M. Baba, "Rotationally resolved ultrahigh-resolution laser spectroscopy of the $S_2\,{}^1A_1 \leftarrow S\,{}^1A_1$ transition of azulene," J. Chem. Phys. **131**, 024303 (2009).

[20] J. S. Baskin, P. M. Felker, and A. H. Zewail, "Purely rotational coherence effect and time-resolved sub-Doppler spectroscopy of large molecules. II. experimental," J. Chem. Phys. **86**, 2483–2499 (1987).

[21] J. Zhan, A. K. Lemmens, M. Ahmed, and M. A. R. Reber, (2026), in Preparation.

Supplemental Materials

V. ADDITIONAL FIGURES

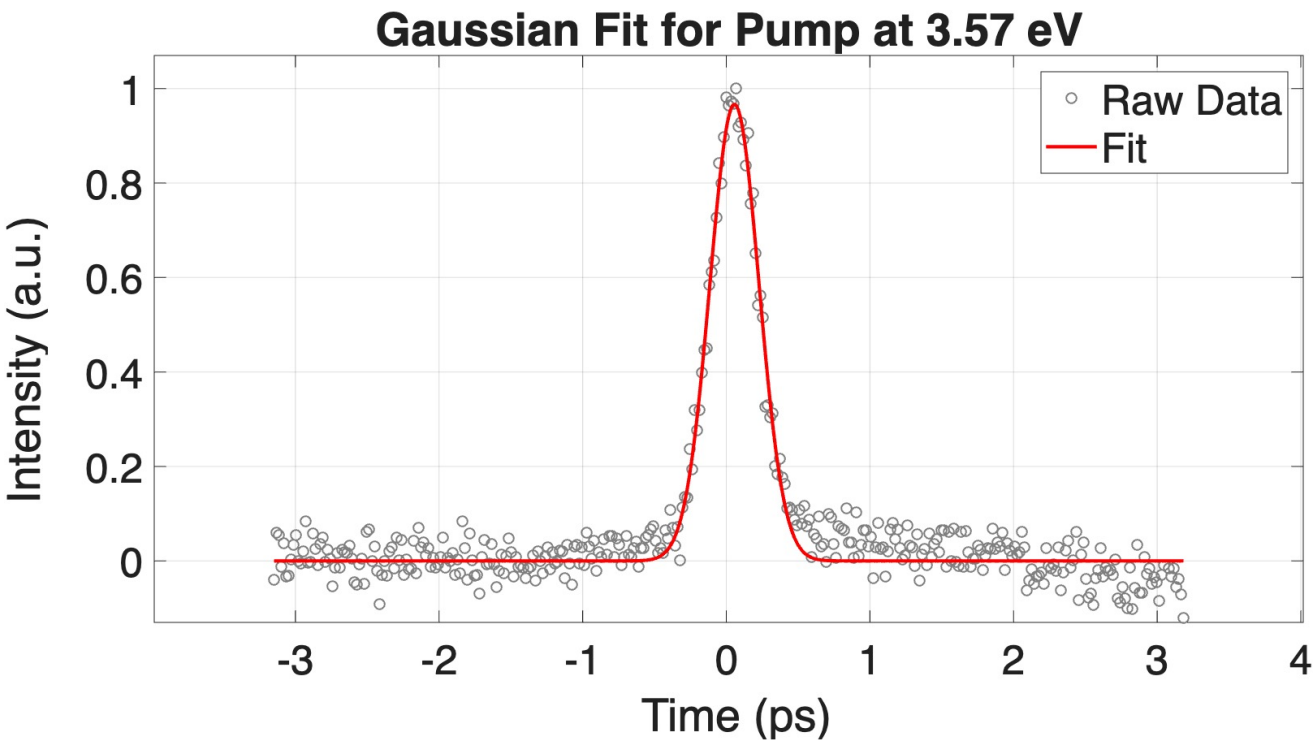

FIG. S1. Gaussian fit for early time dynamics for S_2 azulene when pumped at 3.57 eV. The fitted width is 0.1712 ± 0.0049 ps, corresponding to an FWHM of 0.4032 ps. This FWHM lies within the expected IRF range, indicating the absence of measurable absorption at off-resonance pump energies and demonstrating that the experiment achieves vibronic-state–selective resolution.

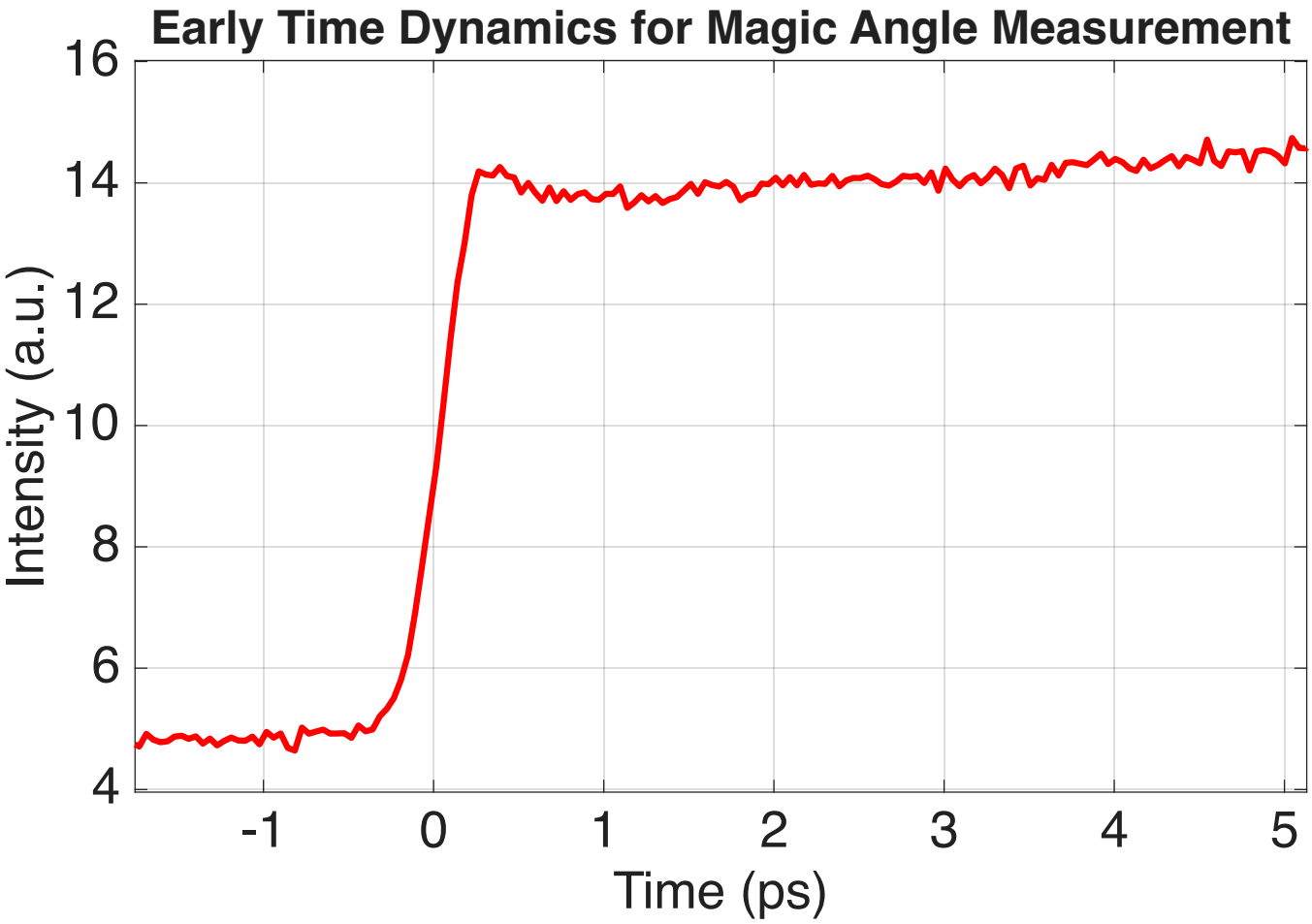

FIG. S2. Raw Data of early time dynamics at magic angle. Pumped at 3.56 eV.

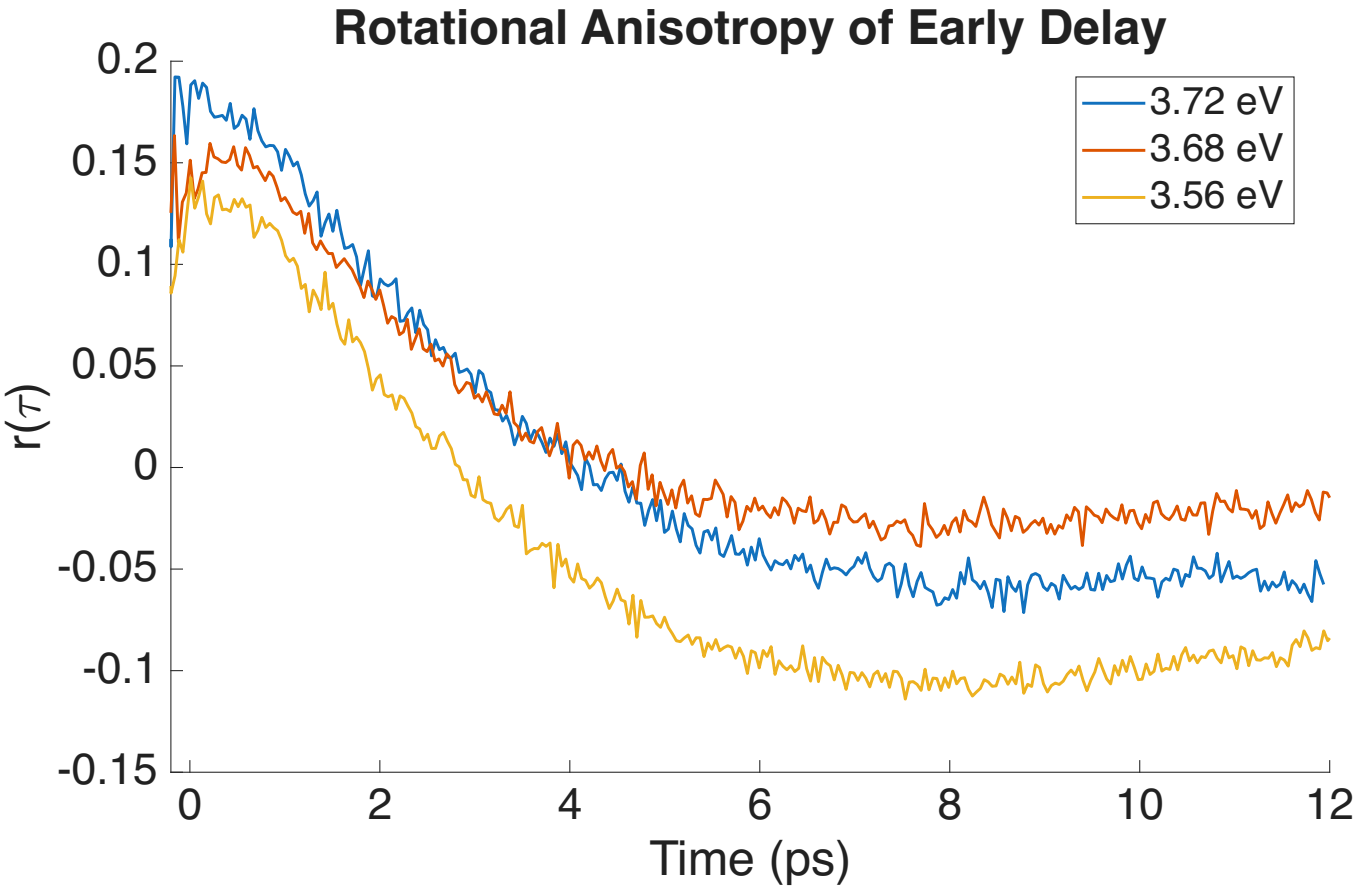

FIG. S3. Rotational anisotropy for pump photon energy of 3.72 eV, 3.68 eV and 3.56 eV. Rotational anisotropy is defined by the following equation: $r(\tau) = \frac{I_{\parallel}(\tau) - I_{\perp}(\tau)}{I_{\parallel}(\tau) + 2I_{\perp}(\tau)}$, where $r(\tau)$ is the anisotropy at a certain time delay, while ($I_{\parallel}$ and $I_{\perp}$ represent the magnitude of the signal with parallel or perpendicular pump polarization, respectively. The maximum value of initial anisotropy $r(0)$ could range from 0.4 to -0.2, depending on the angle between the excitation and detection transition's dipole moments, which can vary from being parallel to perpendicular to each other.

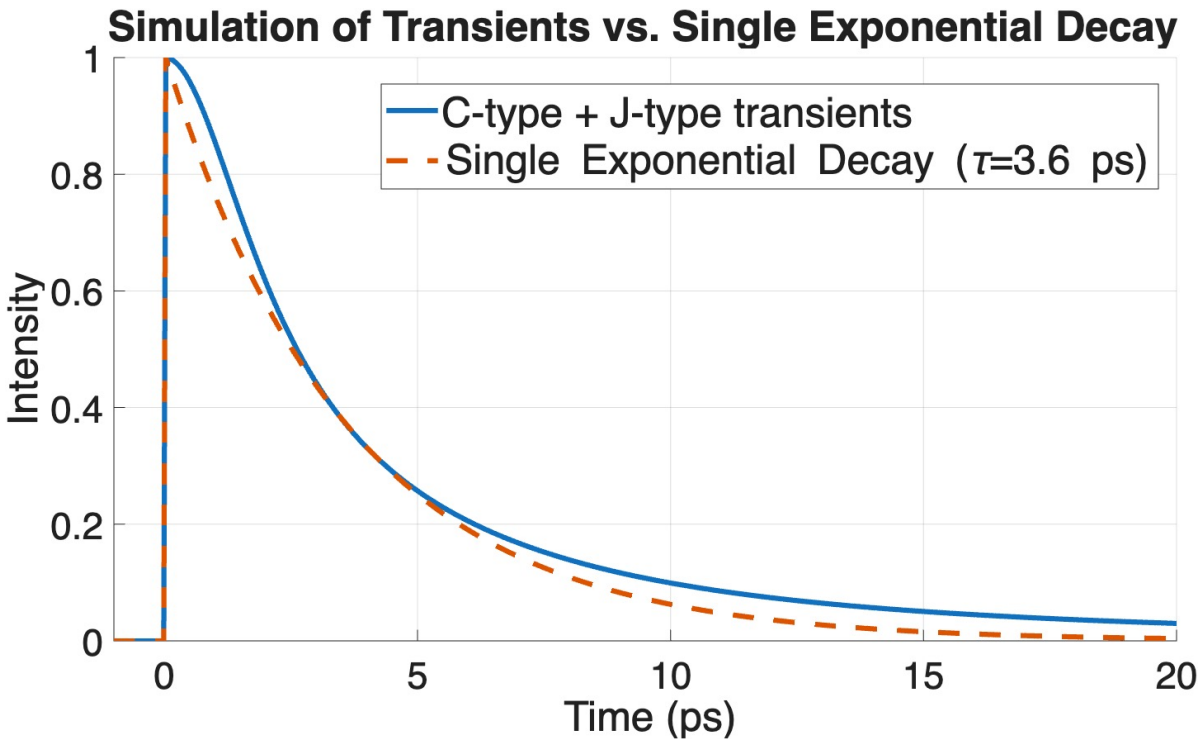

FIG. S4. Simulation of the initial C-type plus J-type rotational coherence dephasing model versus single exponential decay model at early time delay.

VI. SUPPLEMENTARY TABLES

TABLE I. Fitting parameters for scans up to 20 ps using the time-resolved data model Eqs. (1)–(7). The parameter ω_δ represents the width of the coherent artifact (CA). P_2 denotes the amplitude of the initial rotational coherence dephasing term, and τ is the corresponding dephasing lifetime. ω_{irf} represents the fitted instrument response function (IRF) width obtained from the time-resolved model. For photon energies marked with $*$, the reported errors represent half of the difference between the largest upper and the smallest lower bounds of the 95% confidence interval; for all other photon energies, the errors correspond to standard errors.

Photon Energy (eV)	Avg. ω_δ (ps)	error	P_2	error	Avg. τ (ps)	error	Avg. ω_{IRF} (ps)	error
3.56	0.0243	0.0090	0.4733	0.025	3.5669	0.471	0.1727	0.009
3.64$*$	0.0119	0.0017	0.1755	0.025	4.1508	0.503	0.1954	0.005
3.68	0.0098	0.0029	0.3947	0.010	3.4126	0.492	0.1749	0.006
3.70$*$	0.0109	0.0011	0.3487	0.035	3.9916	0.139	0.1776	0.009
3.72	0.0711	0.0406	0.4385	0.022	3.4266	0.404	0.1595	0.010
3.74	0.0388	0.0334	0.3738	0.014	3.1911	0.534	0.1724	0.005
3.77$*$	0.0194	0.0082	0.3713	0.026	4.2631	0.293	0.1994	0.005

TABLE II. Fit parameters for measurements acquired with parallel or perpendicular pump–probe polarization schemes up to 20 ps, analyzed using the time-resolved data model Eqs. (1)–(7). Here, $\parallel$ denotes parallel pump–probe polarization, and $\perp$ denotes perpendicular pump–probe polarization. The parameter ω_δ represents the width of the coherent artifact (CA). P_2 denotes the amplitude of the initial rotational coherence dephasing term, and τ is the corresponding dephasing lifetime. ω_{irf} represents the fitted instrument response function (IRF) width obtained from the time-resolved model. The reported errors represent half of the difference between the upper and lower bounds of the 95% confidence interval.

Polarization	Photon Energy (eV)	ω_δ (ps)	error	P_2	error	τ (ps)	error	ω_{irf} (ps)	error
$\parallel$	3.56	0.0078	0.000	0.5021	0.002	2.5791	0.032	0.1630	0.002
$\perp$	3.56	0.0084	0.000	0.3352	0.002	2.8660	0.060	0.2151	0.003
$\parallel$	3.68	0.0058	0.000	0.3895	0.002	2.3369	0.034	0.1728	0.002
$\perp$	3.68	0.0140	0.000	0.2474	0.002	3.4493	0.086	0.1830	0.003
$\parallel$	3.72	0.0065	0.000	0.4534	0.002	2.6208	0.028	0.1427	0.001
$\perp$	3.72	0.0171	0.000	0.2359	0.005	3.1201	0.171	0.1928	0.003